Exploration Geophysics, Remote Sensing and Environment XXXI.2 (2024)

DOI: 10.26345/EGRSE-017-24-202

ARC-UHI TOOLBOX: A PYTHON-BASED TOOL FOR AUTOMATED MAPPING OF LAND SURFACE TEMPERATURE AND URBAN HEAT ISLAND FROM LANDSAT 9

ARC-UHI NÁSTROJOVÁ NABÍDKA: LANDSAT 9 NÁSTROJ V PYTHONU PRO AUTOMATICKÉ MAPOVÁNÍ POVRCHOVÉ TEPLOTY PŮDY A MĚSTSKÉHO TEPELNÉHO OSTROVA

Sara Sameh[1], Fawzi Zarzoura[2], Mahmoud El-Mewafi[3]

Abstract

ArcGIS is a widely used geospatial data analysis and raster processing software. However, it is not equipped to handle complex data sets and analysis capabilities for certain sensors and camera types compared to other digital image processing programs like ENVI and ERDAS IMAGINE. To overcome this limitation, ArcGIS offers a free framework for programmers to contribute their techniques for enhanced data analysis through modules, tools, or plug-ins. In this regard, researchers developed the Arc-UHI add-in tool using Python programming language for auto-mapping Land Surface Temperature (LST) and Urban Heat Island (UHI) maps from Landsat 9 Collection-2 products. Calculating LST requires time as it involves several computations. The tool simplifies the process and provides all necessary steps and equations for determining LST and UHI using the thermal bands of Landsat 9 images. Cairo city of Egypt was used as a case study to demonstrate the tool's effectiveness. The Arc-UHI tool provides full access to geoprocessing in ArcGIS, a simple graphical user interface, and data processing. The tool's results show that LST and UHI are easily computed for any location using the ArcGIS Add-in Toolbox. The tool's programming code is accessible to the public and can be expanded upon to meet future requirements. The tool will assist users and researchers in focusing more on the study and analysis of data and less on calculations. The LST and UHI tools can also be expanded to provide LST calculations for other Landsat series.

Key words

LST, NDVI, UHI, Python, ArcGIS Toolbox, Landsat 9 Collections.

1. Introduction

Remotely sensed land surface temperature (LST) is usually utilized in meteorological and climatological research, especially for exploring urban heat island (UHI) influence (Sameh et al., 2023). The UHI effect, climate change, rising emissions of greenhouse gases, and other ecological disasters have recently become urgent challenges that need to be handled. The National Aeronautics and Space Administration (NASA) and numerous other global institutions have defined LST and emissivity as major Earth system monitoring collections and crucial climatic variables (Duan et al., 2021). All Landsat satellites provide long-term thermal infrared (TIR) data and using Landsat thermal data to utilize remote sensing information being the most significant areas in an environmental study (M. Wang et al., 2023), Sekertekin and Bonafoni (2020) developed an ArcGIS toolbox for LST calculation, which includes multiple retrieval algorithms and emissivity models, validated against ground measurements, offering valuable insights into LST retrieval from Landsat 5, 7, and 8 over rural areas (Sekertekin and Bonafoni 2020) .

Due to their influence on the urban environment, there has been an increase in research on studying LST and UHIs utilizing multi-temporal thermal satellite images in recent years (A. Al Kafy et al., 2021; Liu et al., 2022; Wang et al., 2017). Landsat images were analyzed to determine brightness temperature (BT) and identify land-use/ Land cover (LULC) according to several biophysical variables (Abdullah et al., 2022). The feasibility of utilizing remote sensing data to assess UHIs based on LST and emissivity values had been investigated in several TIR datasets (Roupioz et al., 2018). Furthermore, the LST of major reconstructed urban districts had been studied in Lyon, France (Renard et al., 2019) and had been associated with other land-use and spectral indices using Landsat data (El-Zeiny & Effat, 2017).

Several studies were conducted in Egypt to better recognize the UHI and its harmful consequences for the ecosystem and humanity. In the case of Egypt's Tanta city, for example, researchers analyzed the UHI growth rates and explored their correlation with different types of LULC (Effat et al., 2014). Additionally, the impact of UHI in Cairo was studied using multiple images from the Landsat satellite. It was discovered that, as the city expanded over agricultural areas, the UHI effect intensified. (Abou El-Magd et al., 2016) . The use of GIS and remote sensing data to measure LST in the El-Fayoum governorate was reviewed (El-Zeiny & Effat, 2017).

This toolbox was developed through a comprehensive process involving several steps. The core of the toolbox was created by coding the UHI mathematical model using the Python programming language. We utilized the PyCharm Integrated Development Environment (IDE) for writing and debugging the Python code, which facilitated the implementation of the UHI and LST calculations.

Once the model was successfully developed and tested in PyCharm, it was integrated into the ArcGIS Desktop environment. This integration was achieved by creating custom Python scripts and tools compatible with ArcMap, which allowed users to perform UHI and

LST calculations directly within the GIS mapping platform. This process ensured that the toolbox operates seamlessly within the ArcGIS ecosystem, leveraging its mapping and spatial analysis capabilities.

ArcGIS poses a challenge in research because it lacks robust image processing capabilities for specific sensor models. This limitation can complicate the integration of research findings and necessitate the use of multiple software applications, causing workflow disruptions. While alternatives like ENVI and ERDAS IMAGINE offer advanced image processing, but they come at a cost and require licensing. To address this issue in a research context, customized image processing tools have been developed within the ArcGIS environment using ArcPy. These tools provide support sensor models that ArcGIS doesn't naturally accommodate, eliminating the need for external software and enhancing the research integration process. These tools have been developed to enable automatic calibration and estimation of temperature values from Landsat 9 collection-2 (C2) OLI and TIRS. This is particularly relevant as of January 1, 2022, since the forward processing of Landsat Collection-1 (C1) has terminated. Landsat C2's Level-1 (L1) and Level-2 Science Products (L2SP) offer updated data distribution procedures and radiometric, geometric, and precision/terrain corrections (Wulder et al., 2019).However, there is currently no availability of Level-2 products for Landsat MSS 1-5 data.

In ArcGIS 10.6, a spectral radiance model is employed to investigate urban vegetation loss and its impact on LST (A.-A. Kafy et al., 2021). Kim et al. propose using the Arc-Mine tool, which is a plug-in for ArcGIS, to plan restoration in abandoned mined areas by examining mine subsidence, mine waste abrasion calculation, mine water flux route determination, and tree species suitability analysis for coal mine forestation (Kim et al., 2012). Hakan OĞUZa (2016) used the Visual Basic.NET programming language to develop a software tool that derived LST from Advanced Space-borne Thermal Emission and Reflection Radiometer (ASTER) imagery (Oguz, 2016). The LST calculation model was designed using the ArcGIS model builder to minimize calculation time (Khan et al., 2022). An additional ArcGIS Desktop 10 toolbox for automatic retrieval of BT Map, land surface emissivity (LSE), and LST using the single channel algorithm has been presented (J. P. Walawender et al., 2012).

Determining LST heterogeneity is a complex and meticulous process that demands precise calculations. Scientists need to be aware of all the formulas and constant values before performing any calculations. Based on a review of several research publications, it has been discovered that researchers are using the traditional approach for calculating LST, which is time-consuming and demands accuracy. Various studies use programming language codes to create various add-in tools in ArcGIS, so an Arc-UHI Add-in Toolbox was created in this study to reduce the effort of repetitive raster calculation and make it easier and faster. The main objective of this study is:

- Our study develops Arc-UHI, a Python-based add-in tool for ArcGIS that simplifies the computation of LST and UHI maps from Landsat 9 Collection-2 products, addressing ArcGIS limitations for advanced data processing.
- Automatically converting data from Landsat 9 products into different maps, such as spectral radiance, reflectance, and temperature, and then using that data to calculate normalized difference vegetation index NDVI, LSE, and surface temperature.
- Assure that LST and UHI data are generated as quickly as possible.
- Reduce the time, it takes to re-enter equations for various computations done during the LST and UHI calculations,
- Design a tool that can generate multiple maps from fewer procedures.

2. Study area

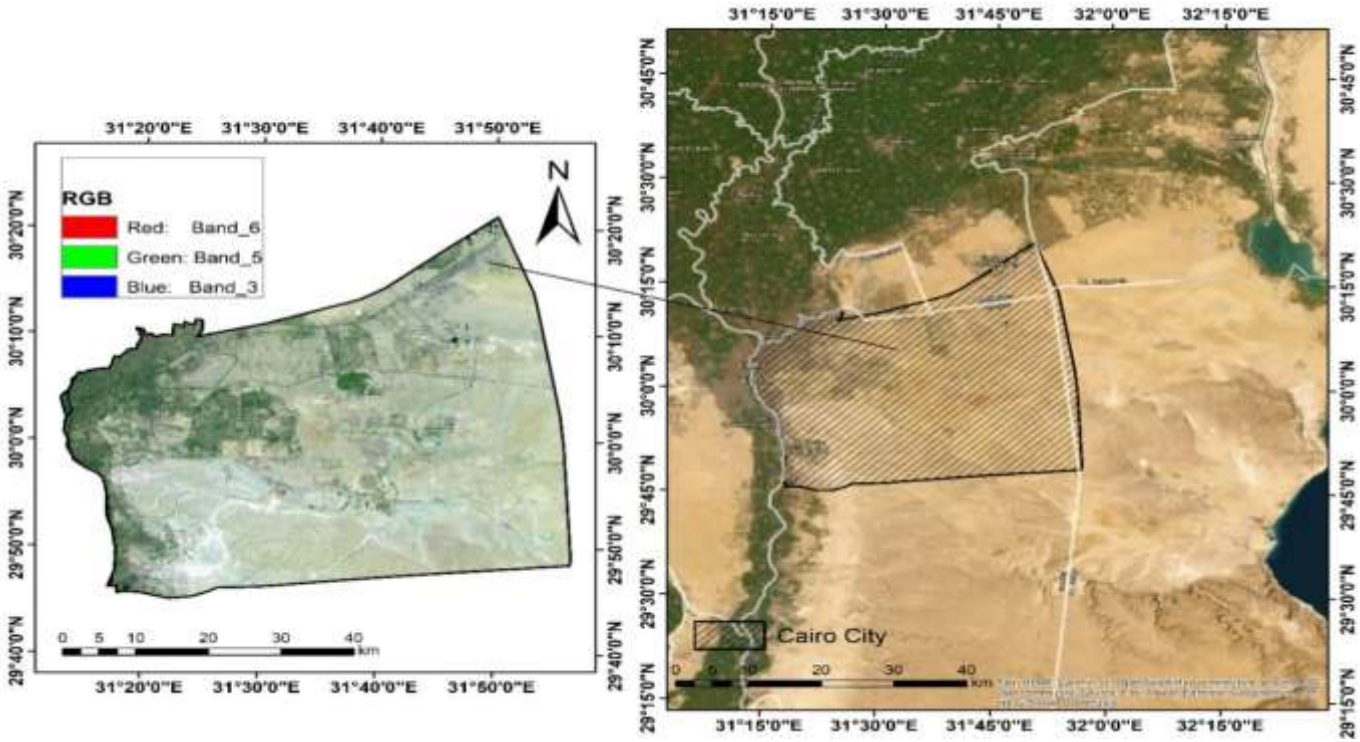

The Arc-UHI tool was created to calculate LST and detect UHI. The largest metropolis in Egypt, Cairo, has been chosen as the research region to demonstrate the Arc-UHI Calculator toolbox. Egypt's capital, Cairo, is the sixth-largest metropolitan area globally and the biggest city in Africa, the Middle East, and the Arab world, as shown in Fig. ***1***. It has a total population of 21.9 million people, an area of 3124.7487 km2, and a density of population of 17601/km2.The rapid growth of Cairo's urban areas and population has caused a shift in land use from original state to artificial surfaces that absorb heat, resulting in high Land Surface Temperatures (LST).This has resulted in a significant UHI effect in Cairo.

Fig. 1: Landsat 9 scene of Cairo, Egypt, used for the application of the Arc-UHI tool

3. Materials and methods

This research used a method known for its simplicity and effectiveness in LST retrieval. Numerous investigations have been conducted to assess the accuracy of various algorithms in LST computation. A separate study corroborated these outcomes, highlighting the Mono-Window algorithm's superiority in terms of accuracy and precision over other available methods.

The Arc-UHI toolbox in ArcGIS 10.5 was created using the Python 3.6 programming language. The Arc-UHI add-in toolbox utilizes a variety of equations that were certified by the USGS. The Arc-UHI Tool makes use of a Landsat 9 C2 L1 and C2 L2SP bands scene (path/row: 176/39), acquired on August 20, 2022, and downloaded from Earth Explorer (https://earthexplorer.usgs.gov/).

Landsat 9 satellite, launched in September 2021 by NASA and the USGS, is equipped with two sensors that enable continuous Earth observations for the next five years Landsat 9 is only available in C 2 (United States Geological Survey (USGS), n.d.-a). The satellite's radiative transfer equation technique is used to generate Landsat 9 C2 L2SP LST data, which can be useful for studying UHI. The Landsat 9 LST product has been found to perform well in initial validation, and the split-window algorithm may be the preferred method for retrieving LST from Landsat 9 data due to the TIRS-2 sensor's capability to handle stray light (Hulley et al., 2021).

The Landsat 9 satellite continues the Landsat program's objective of surveying, evaluating, and overseeing land resources vital for human survival. The satellite carries two science instruments, the Operational Land Imager 2 (OLI-2) and the Thermal Infrared Sensor 2 (TIRS-2). Landsat 9 imagery was downloaded in 11 bands.

4. Design and implementation of the Python Tool: UHI Calculator for ArcGIS Desktop

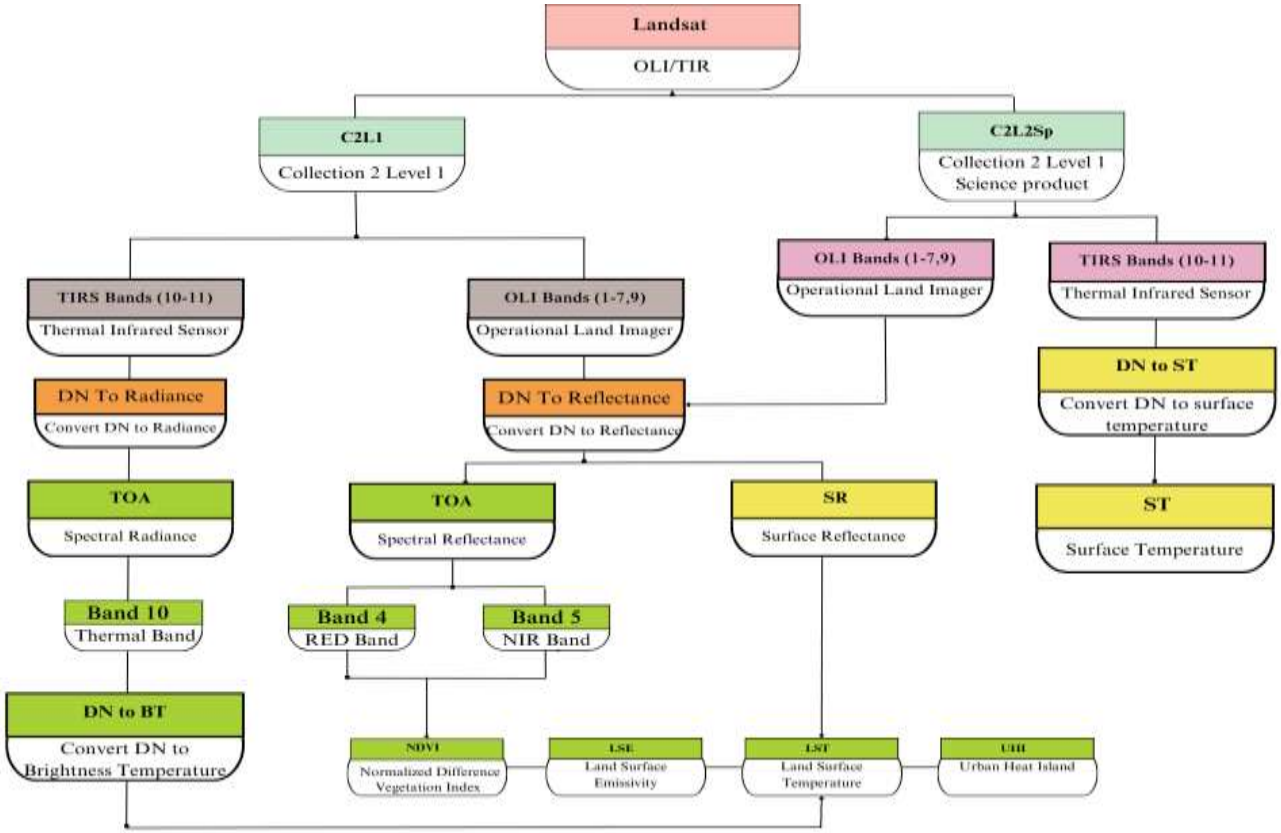

Fig. 2: Methodology for radiometric calibration and LST calculations

This toolbox is compatible with ArcGIS Desktop, ESRI's GIS mapping platform, and was developed using the Python programming language. The process for calibrating Landsat 9 OLI/TIRS C2 L1, and C2 L2 products and estimating land surface temperature from the TIRS band is illustrated in Figure 2. This figure depicts the methodology and workflow of various tools created specifically for this study. The Arc-UHI toolbox is divided into two individual toolsets Figure 3. The explanation for these toolsets is detailed in the next section.

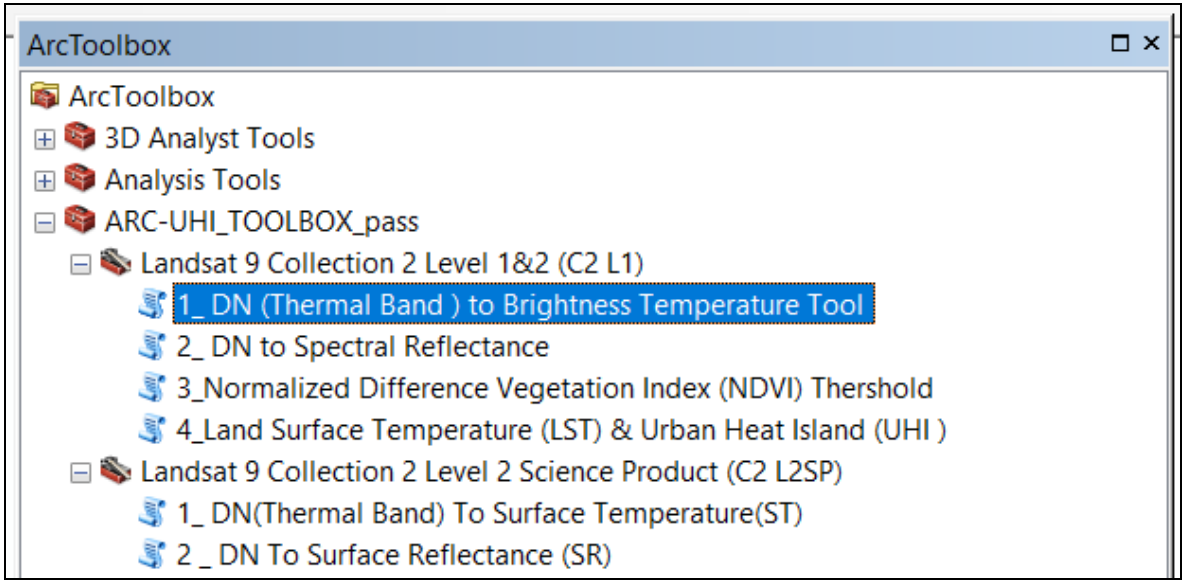

Fig. 3: Arc-UHI Add-in Toolbox toolset

4.1. Convert thermal band digital number (DN) to brightness temperature tool

Landsat imagery includes TIR sensors that record the temperature of the area being captured; LST and UHI are calculated using satellite thermal bands. Various Landsat packages have several thermal bands; for our research, Landsat 9 was selected, which includes two thermal bands. Based on the USGS, thermal band 10 provides superior results and less ambiguity for surface radiance than band 11 (United States Geological Survey (USGS), n.d.-b), so band 10 would only be used in this study.

The tool's first step is to use Eq.1 to transform the image pixels of band 10 of the Landsat thermal band's Digital Numbers (DNs) to spectral radiance(L_λ). After that, it converts L_λ to BT by the inverse of Planck's law and a particular thermal conversion constant determined from metadata, as given in Eq. 2. (Ihlen, 2019):

$$L_\lambda = \mathrm{ML} * Q_{cal} + \mathrm{AL} \qquad (1)$$

$$BT = \frac{K_2}{\ln\left(\frac{K_1}{L_\lambda}+1\right)} - 273.15 \qquad (2)$$

where, L_λ refer to spectral radiance (Wm-2×sr-1 × μm-1), ML is a coefficient that scales the thermal band's radiance multiplicatively, AL is the additive scaling factor of radiance for a thermal band and Q_{cal} is the digital number value of the thermal band, and for Eq. 2, BT refers to Brightness temperature in (°C), K1 and K2 are the constants used to convert the thermal values from the metadata.

4.2. Convert DN to spectral reflectance

The presented tool facilitates the conversion of data obtained from the Landsat 9 C2 OLI sensor into both spectral and surface reflectance by applying the scaling factors specified in the metadata file using Eq.3. The Landsat Surface Reflectance Code (LaSRC) algorithm is used to eliminate the impacts of atmospheric particles on the light absorption and scattering in C2 L2SP.

$$\rho_\lambda' = M\boldsymbol{\rho} * Q_{cal} + A\boldsymbol{\rho} \qquad (3)$$

where ρ_λ' is refer to spectral reflectance, before sun angle correction, for data from Landsat 9 C2 L1 and it also refers to surface reflectance from Landsat 9 C2 L2SP, M$\boldsymbol{\rho}$ is the scaling factor specific to the band and is used to scale reflectance, Q_{cal} is the input DN L1 pixel values of the band and A$\boldsymbol{\rho}$ is the specific reflectance additive scaling factor for bands (1-7,9).

The ρ_λ' generated from L1 data is not correct spectral reflectance due to the absence of a correction for sun elevation angle. Here is Eq. 4 for calculating spectral reflectance.

$$\rho_\lambda = \frac{\rho_\lambda'}{\sin\theta_{SE}} \qquad (4)$$

where ρ_λ is sun elevation correction spectral reflectance, θ_{SE} is scene-center sun elevation angle in degrees. the toolset calculates corrected spectral reflectance using the scene-center solar elevation angle from the metadata file. L2SP products do not incorporate the solar elevation angle at the scene center as a parameter in the data processing algorithm (Vermote et al., 2016).

4.3. NDVI thresholds tool

The tool estimates the LSE map using a theoretical model relating emissivity based on NDVI thresholds. This index is dependent on the radiative properties of chlorophyll, which strongly absorbs visible light in the process of photosynthesis, as well as on the structure of leaf cells, which strongly reflect radiation in the near-infrared range. The NDVI provides information on green vegetation cover (Tucker, 1979). In the case of Landsat 9 images, NDVI is derived by combining Band 4 and Band 5 spectral bands using Eq. 5.

Hence, determining the NDVI is critical (Sameh et al., 2023). The NDVI must be calculated because the fractional vegetation index (FV) must be estimated thereafter; the FV and the NDVI are inextricably linked. Emissivity (ε) is also necessary to calculate and is related to FV.

$$NDVI = \frac{NIR-RED}{NIR+RED} \quad (5)$$

The value of the near-infrared band is represented by NIR, while the value of the red band is represented by RED.

Fractional vegetation monitoring measures the space filled by trees, branches, and leaves in proportion to the total vegetation region. We require NDVI to calculate fractional vegetation Eq.6. The maximum and minimum values of NDVI are taken from an NDVI map created with Eq.5.

$$FV = \left(\frac{NDVI-NDVI_{min}}{NDVI_{max}-NDVI_{min}}\right)^2 \quad (6)$$

The proposed model categorizes pixels based on their NDVI values, with NDVI values less than 0.1 being considered bare soil with an emissivity of 0.96, NDVI values greater than 0.72 being considered fully vegetated with a vegetation cover of 1, and an emissivity of 0.985, and NDVI values between 0.1 and 0.72 being considered as spectrally mixed pixels. The emissivity of the surface for spectrally mixed pixels is determined using Eq. 7. (Valor & Caselles, 1996):

$$\begin{cases} NDVI < 0.1, & \varepsilon_s = 0.96 \\ 0.1 \le NDVI \le 0.72, & \varepsilon = \varepsilon_v F_v + \varepsilon_S (1 - F_v) + d_\varepsilon \\ NDVI > 0.72, & \varepsilon_v = 0.985 \end{cases} \quad (7)$$

where ε is land surface emissivity, ε_V is the emissivity of full vegetation, ε_s is the emissivity of full soil and d_ε refer to the roughness of the surface, which may be insignificant for land with flat surfaces $(d_\varepsilon = 0)$, though, for rough surfaces with a value of 2%, Eq. (8) can be used to calculate it (Sobrino et al., 1990):

$$d_\varepsilon = (1 - \varepsilon_s)(1 - FV)F\varepsilon_V \quad (8)$$

and F is the Shape factor (Sobrino et al., 1990), considering various geometrical distributions, is 0.55 (Sobrino et al., 2004)

4.4. Land surface temperature from C2 L1 and surface temperature from C2 L2SP

According to Eq. 9, the tool for deriving LST relies on a methodology developed for the Landsat data. Previous studies (Walawender & Hajto, 2009) have examined the benefits of using Landsat images to calculate LST trends in metropolitan regions. LST determined using satellite TIR data has frequently been regarded as a significant indicator for understanding the spatial impacts of UHI.

$$LST = \frac{BT}{1+(\frac{\lambda * BT}{\rho})} * \ln \varepsilon \quad (9)$$

in which, h is Planck's constant = $6.626*10^{-34}$ J s, c is light's velocity = $2.998*10^{8}$ m/s and S is the constant of Boltzmann = $1.38 * 10\text{-}^{23}$ J/K, $\rho = \frac{h*c}{s} = 1.438 \times 10^{-2}$ m and λ is the wavelength of the radiation emitted and Ɛ is land surface emissivity.

To generate the Surface Temperature (ST) raster, each pixel value of the thermal band from Landsat 9 C2L2SP used information from the metadata, including a scale factor and offset value per pixel. The resulting ST raster contains temperature values in Celsius (Wulder et al., 2022).

4.5. Urban heat island

To assess the LST or ST of an area with the surrounding areas, a normalization procedure was used in Eq. 10 to calculate UHI (Abutaleb et al., 2015):

$$UHI = \frac{T_s - T_m}{SD} \quad (10)$$

where, T_s , Tm indicates to LST and the mean LST of the study region, respectively, and SD is the standard deviation.

Following the initial development and integration of the Arc-UHI Toolbox, its functionality was carefully tailored to meet the needs of urban climate research. The toolbox, integrated into ArcGIS Desktop, facilitates automated LST and UHI calculations through its Python-based algorithms. Key features include a user-friendly interface that simplifies access to its functionalities, thereby enhancing workflow efficiency and reducing the likelihood of errors associated with manual calculations. The toolbox's compatibility with ArcGIS Desktop ensures that it leverages existing GIS tools for data analysis and visualization, providing seamless integration into users' established workflows. Practical applications of the toolbox have been demonstrated in several case studies, where it has effectively analyzed urban heat islands in diverse urban environments. These applications showcase the toolbox's capability to handle complex data sets and generate valuable insights into temperature variations and vegetation impacts.

5. Result and discussion

The ArcGIS add-in tool is created to perform automated mapping to Landsat 9 C2L1 and C2L2Sp images. In this research, we build upon previous studies that utilized ArcGIS to investigate various aspects of the loss of urban vegetation (A.-A. Kafy et al., 2021), mine restoration planning (Kim et al., 2012), and land surface temperature (LST) estimation (Oguz, 2016). The analysis demonstrates that the toolbox effectively automates UHI and LST calculations, significantly improving efficiency and accuracy compared to manual methods. The results illustrate the toolbox's successful integration with GIS platforms, providing a practical solution for urban climate research.

These findings highlight the toolbox's potential to enhance the analysis of urban heat islands and land surface temperatures in diverse urban environments. By addressing the limitations of ArcGIS for advanced data processing, our research offers a valuable tool that significantly reduces the effort required for repetitive raster calculations, enabling faster and more efficient analysis. This research has the potential to enhance the accuracy and accessibility of LST and UHI mapping, supporting urban planning and environmental management efforts. In areas with water bodies, the correlation between NDVI and LST values differs significantly from that observed in other land cover types. Water bodies, due to their unique thermal properties, tend to have low NDVI and low LST values. This is because water heats up and cools down more slowly than land, resulting in lower surface temperatures. In contrast, other land cover types, such as bare soil or sparsely vegetated areas, typically exhibit low NDVI values that correspond to higher LST due to the direct exposure of the surface to sunlight. It is important to highlight this distinction in our analysis, as the presence of water bodies can lead to deviations from the general NDVI-LST relationship observed in terrestrial environments. Understanding this contrast is crucial for accurately interpreting the spatial variability of LST in regions with mixed land cover.

5.1. Calculation of spectral radiance and brightness temperature

This tool in the Arc-UHI toolbox aims to transform the DN of a thermal band from Landsat 9 C2 L1 into a Spectral radiance after that from a spectral radiance map getting a brightness temperature map Figure 4. In the data that is downloaded with the satellite bands, you can find the ML and AL parameter values that are needed as input in this tool. In addition, a metadata file is used to derive the thermal constants' (K1, K2) values. The constant values for each Landsat series are contained in a separate metadata file; the constant values for Landsat 9 are shown in Table 1. The TIRS band 10 was calibrated to estimate spectral radiance ($L\lambda$) and brightness temperature maps for Cairo city as a case study (Figure 5). The spectral radiance ($L\lambda$) map values range between 9.5886 and 12.6271 and they are consistent with the LEVEL1_MIN_MAX_RADIANCE value range specified in the downloaded data file of Landsat 9 C2 L1. The RADIANCE_MAXIMUM_BAND_10 is 25.00330 and the RADIANCE_MINIMUM_BAND_10 is 0.10038.

5.2. Calculation of spectral and surface reflectance

To obtain the LST, a radiometric correction is performed on every Landsat 9 C2L1 band that is inputted. This correction is necessary to accurately measure the temperature of the land surface. The raw digital numbers (DNs) from the OLI bands are transformed into spectral reflectance and surface reflectance by rescaling them (Figure 6). This conversion is necessary to make the data more useful and accurate for analysis. Table 1 display the rescaling factors for each band and other constants, which can be found in the metadata file that was downloaded that was needed as input data in these tools. Figure 7 (a and b) depicts the range of spectral reflectance values for bands 4 and 5, with values varying between 0.05922 and 0.59974 for band 4 and between 0.0336 and 0.73772 for band 5. It is noteworthy that both these ranges are within the value range of LEVEL1_MIN_MAX_REFLECTANCE mentioned in the metadata file of Landsat 9 C2L1. The Surface Reflectance maps for bands 4 and 5 are represented in Figure 7 respectively.

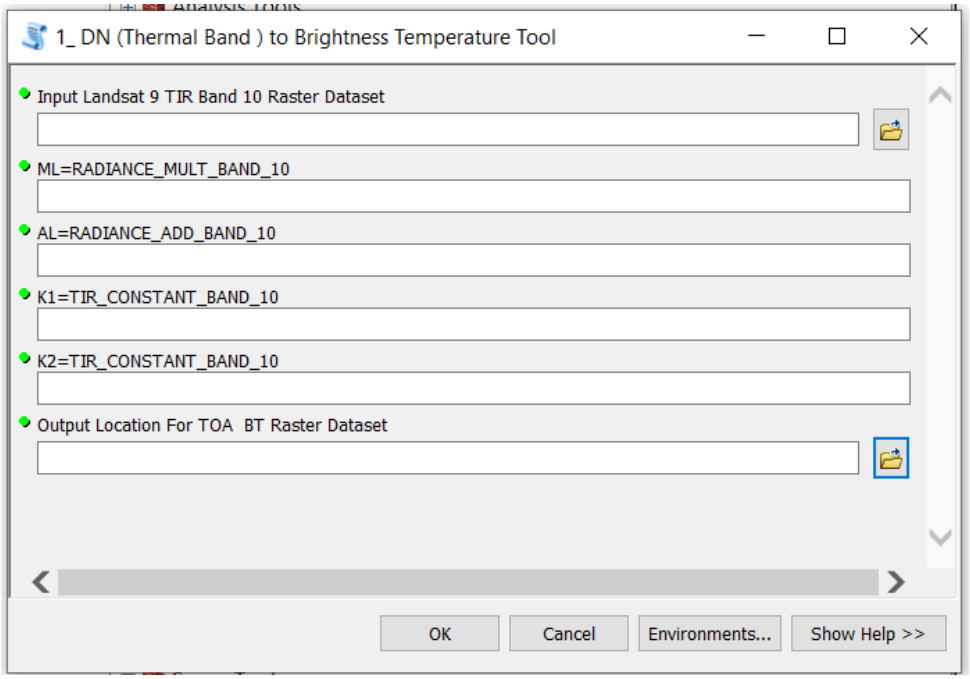

Fig. 4: Tool interfaces of Arc-UHI toolbox to convert DN (Thermal Band) C2 L1 to brightness temperature

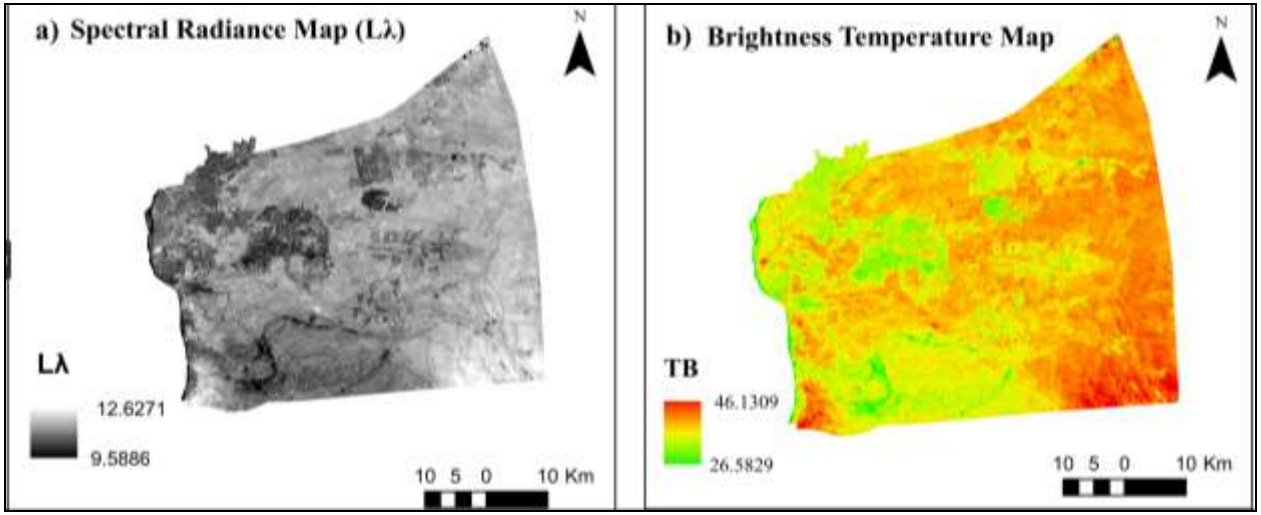

Fig. 5: Output raster datasets derived from the first tool: Spectral radiance and BT for the TIRS 10 band maps

Tab. 1: The constants for Landsat 9 used in Arc-UHI Tool

Constants	Definition			Value
K_1	K1_CONSTANT_BAND_10	Landsat 9 C2 L1	TIR band 10	799.0284
K_2	K2_CONSTANT_BAND_10			1329.2405
ML	RADIANCE_MULT_BAND_10			0.00038
AL	RADIANCE_ADD_BAND_10			0.1
Aρ	REFLECTANCE_ADD_BAND_X		OLI band (1-7,9)	-0.1
Mρ	REFLECTANCE_MULT_BAND_X			0.00002
θ_{SE}	SUN_ELEVATION			62.24701632
ML	TEMPERATURE_MULT_BAND_ST_B10	Landsat 9 C1 L2SP	TIR band 10	0.000341802
AL	TEMPERATURE_ADD_BAND_ST_B10			149
Aρ	REFLECTANCE_ADD_BAND_X		OLI band (1-7,9)	-0.2
Mρ	REFLECTANCE_MULT_BAND_X			0.0000275

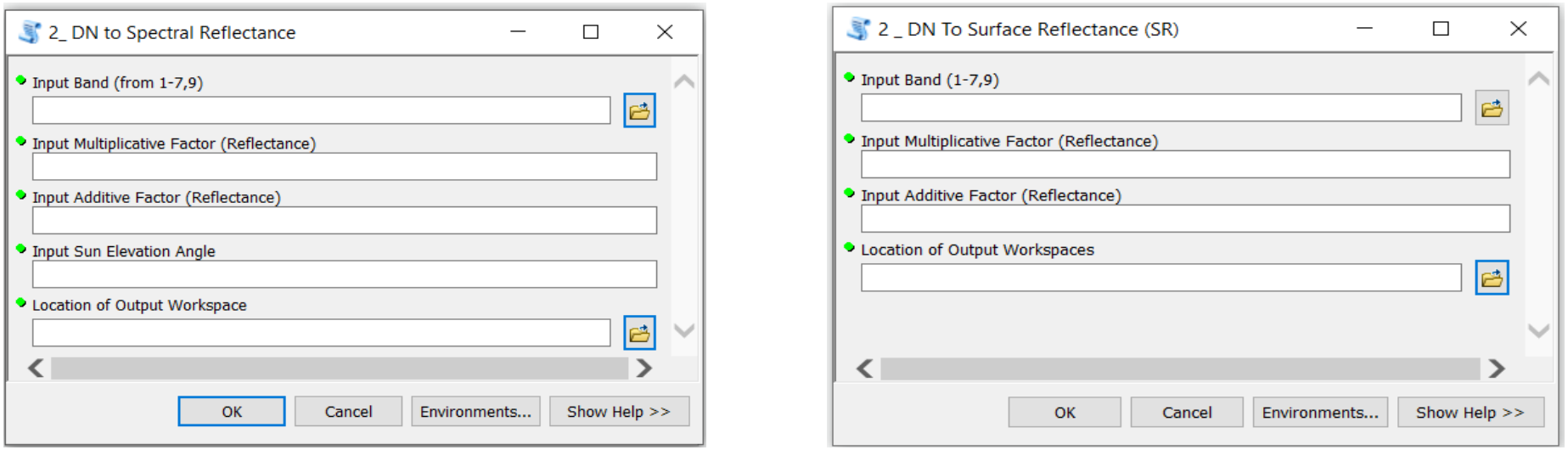

Fig. 6: Tool interfaces of Arc-UHI toolbox: DN to spectral reflectance tool (C2L1) and DN to surface reflectance (SR) tool for (C2 L2SP)

5.3. Calculation of NDVI and emissivity

The Landsat 9 satellite is used to obtain spectral reflectance values through the rescaling of raw DN data, with bands 4 and 5 as used for radiometric correction and NDVI calculation. The Arc-UHI toolbox is utilized to obtain NDVI, FV, and ε maps as shown in Fig. *7*, which are used to classify different earth surface features. NDVI values range from -1 to 1 and are used to determine the proportion of vegetation in an area. The FV value represents the proportion of vegetation, while ε indicates the emissivity of different land covers in Cairo city presented in Fig. .

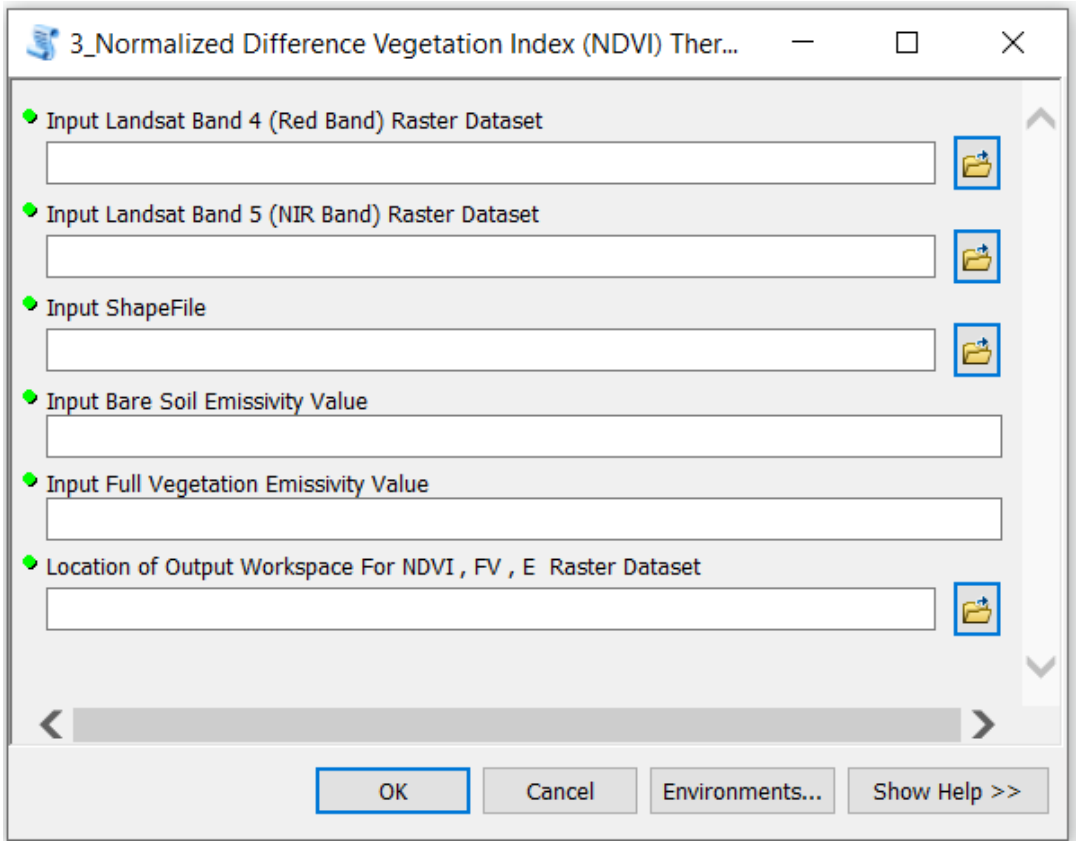

Fig. 7: Tool Interfaces of Arc-UHI toolbox: Normalized difference vegetation index(NDVI) tool

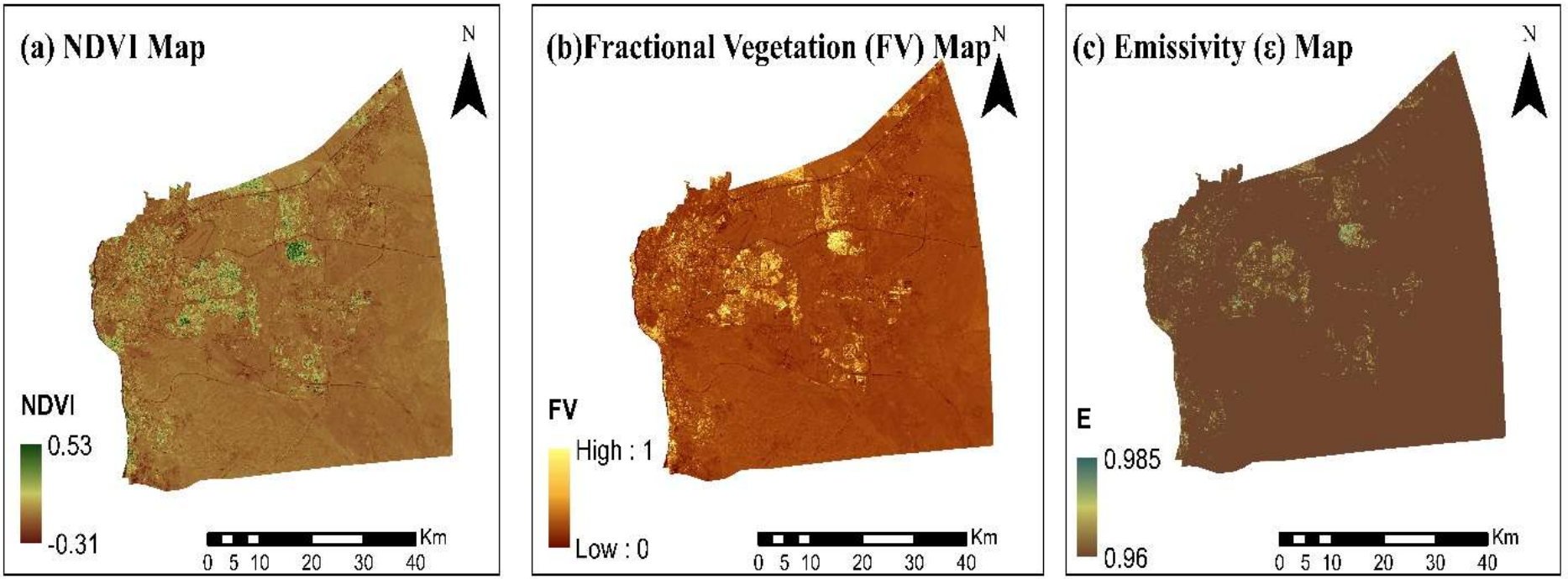

Fig. 8: Output Raster datasets: NDVI map, fractional vegetation map and emissivity map

5.4. Calculate Land Surface Temperature and Surface Temperature Tools.

Arc-UHI tool was used to estimate the geographical distribution of LST for the Landsat 9 C2 L1 image and the ST distribution map for Landsat 9 C2 L2SP. Finally, the user can calculate the LST using BT and emissivity maps, which can be provided by the previous tools, or any other algorithms to calculate emissivity, as shown in Fig. 9: Tool interfaces of Arc-UHI toolbox: LST &UHI tool and DN to ST (C2L2SP) Tool

Fig. depicts the final spatial distribution of LST and UHI maps that were relative using this tool in the toolbox. The minimum and maximum temperatures of the scene were computed as 26.61 ºC and 46.2 ºC. Fig. (b) shows an LST map of Cairo, Egypt, showing very high spatial variability in LST. As expected, high temperatures were retrieved within UHI zones, as shown in Fig. (c).

The ST map can be provided from Landsat 9 C2 L2SP using the Arc-UHI toolbox. As shown in Fig. (a), the required input is the thermal band in addition to multiplicative and additive factors which can be obtained from the metadata file downloaded with Landsat 9 C2 L2SP inserted in Table 1.

Using the created tools, time-series LST or UHI may be quickly and easily calculated for any chosen region of the world using any Landsat 9 C2 data for various seasons within the ArcGIS Environment. The process of estimating LSE or LST from Landsat 9 C2 products

is made easier with the use of the Arc-UHI toolbox for ArcGIS Desktop. There is no need for manual calculation using Raster Calculator. Simply download the Landsat 9 C2 products from the Earth Explorer (EE) site and use the developed toolbox to calibrate the images and retrieve the radiometrically corrected results.

The Arc-UHI plugin add-in toolbox allows users to specify a location for saving each output file generated by the tool. The user can choose to save the maps to the same or different workspace locations. The Arc-UHI Tools are freely available for scientific use.

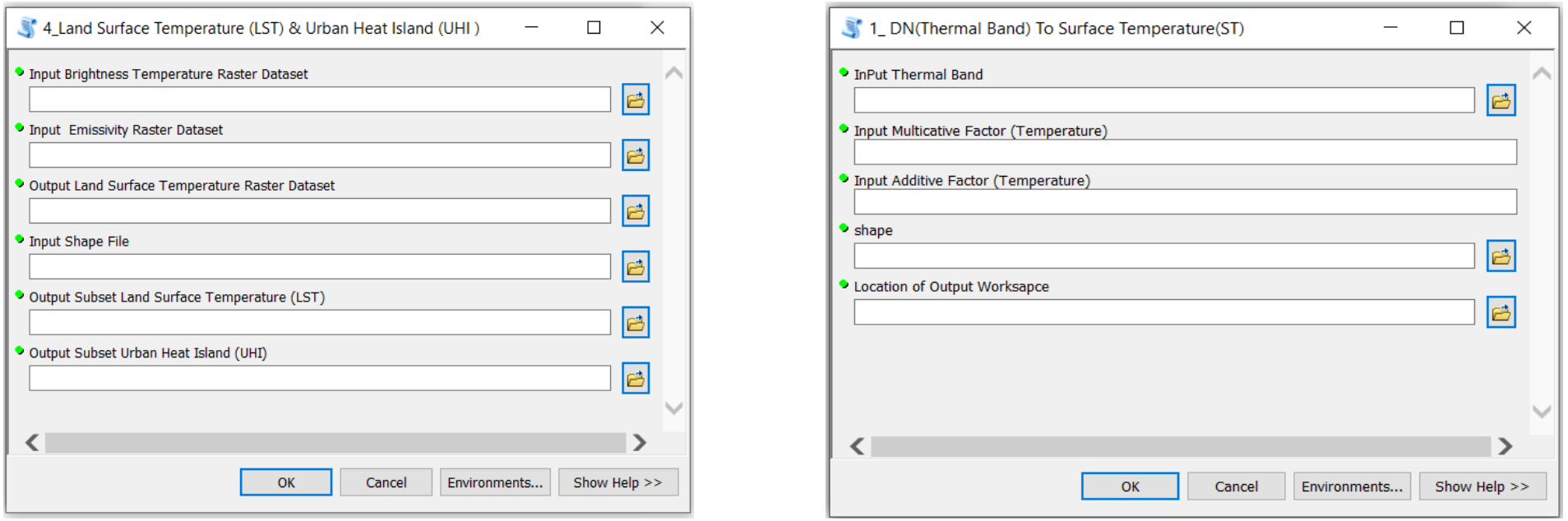

Fig. 9: Tool interfaces of Arc-UHI toolbox: LST &UHI tool and DN to ST (C2L2SP) Tool

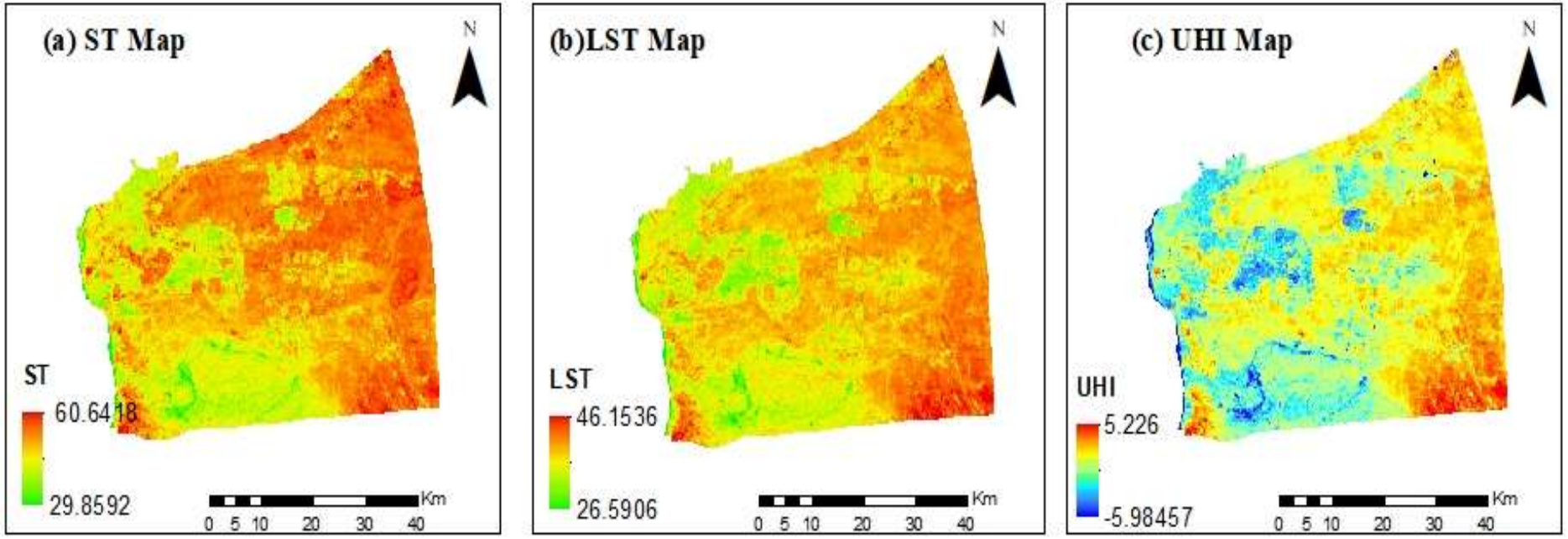

Fig.: 10 Output raster datasets derived from the third tool: (a) ST from C2 L2SP, (b) LST from C2 L1map and (c) UHI map

5.5. Arc-UHI Toolset Validation

Validation and testing is a crucial part of the software/tool development process since it increases the tool's reliability and user adoption. All of the created tools' results are cross-checked against Landsat 9 C2 L2SP Products, LULC, and NDVI to ensure accuracy and precision. The L2SP are ready-to-use products that have undergone research-level processing and are generated from Landsat L1 OLI/TIRS data. They consist of Landsat surface reflectance (SR), ST, and provisional aquatic reflectance for Landsat 9. Digital numbers (DNs) are 16-bit unsigned integers that range from 1 to 65,457 and are used to represent the Landsat 9 L2SP products acquired for the same location and date as the data from Landsat 9 C2L1.

To use the data for validation purposes, it is crucial to convert the raw DN values into meaningful surface reflectance (SR) and surface temperature (ST) values using a scale factor. The Radiometric Calibration toolset offers two tools, namely the DN to Reflectance and DN to Surface Temperature (C2 L2SP), which can be utilized to perform the conversion. These tools are necessary for rescaling the raw DN values into their corresponding physical values, which are required for validation purposes.

Validation of Arc-UHI with C2 L2SP products

For the validation of data, maximum and minimum reflectance and temperature values obtained from both C2 L1 and C2 L2SP are utilized. Among these, C2 L2SP products are preferable for validation purposes as they have undergone atmospheric correction, which enables them to provide more actual values of surface reflectance and temperature. The C2 L2SP SR and ST data are used to establish the variance, as depicted in Fig.a The variance in SR is negative, indicating that the range of values in C2 L2SP is greater than that in C2L1, while the deviation in ST is positive, as shown in Table 2.

Tab: 2. Validation data derived from C2 L1 with data from C2 L2SP

	Surface Reflectance				Surface Temperature (ST)	
	Red Band		NIR Band		Thermal Band (B10)	
	Minimum	Maximum	Minimum	Maximum	Minimum	Maximum
C2 L1	0.05922	0.59974	0.0336	0.73772	26.5906	46.1536
C2 L2SP	0.0275625	0.704888	0.0203025	0.831745	29.8592	60.6418
Variance	-0.0316575	0.105148	-0.010575	0.094025	3.2686	14.4882
Average Variance	-0.015416875		-0.026287		1.31715	

The reason for this difference can be attributed to the constraints of C2L1 products, as they are susceptible to the impact of atmospheric gases and aerosols causing scattering and absorption effects. Small variations in calibrated surface reflectance and estimated LST obtained from (C2L1) products were taken into account and utilized in the study. Although there is a noticeable asymmetry between the estimated land surface temperature (LST) values from C2L1 and the rescaled C2 L2SP surface temperature (ST) values obtained using the developed tools, the two datasets still exhibit similar trends and relationships. These similarities are demonstrated through the results, histograms, and scatter plots in Fig. and

Fig. , which provide additional support for the accuracy of our findings. However, it should be noted that there is a significant difference in the value range of LST between C2L1 and C2 L2SP. the difference in LST values obtained from C2L1 and C2L2SP data products. The C2L2SP product is processed using auxiliary atmospheric data, including ASTER, emissivity, NDVI, and GEOS atmospheric profiles, which 394 enhances its flexibility in handling various datasets and generating additional layers like NDVI, 395 LSE, radiance, and reflectance. The difference in LST values obtained from these two products is significant, but the trends and relationships in the data remain comparable.

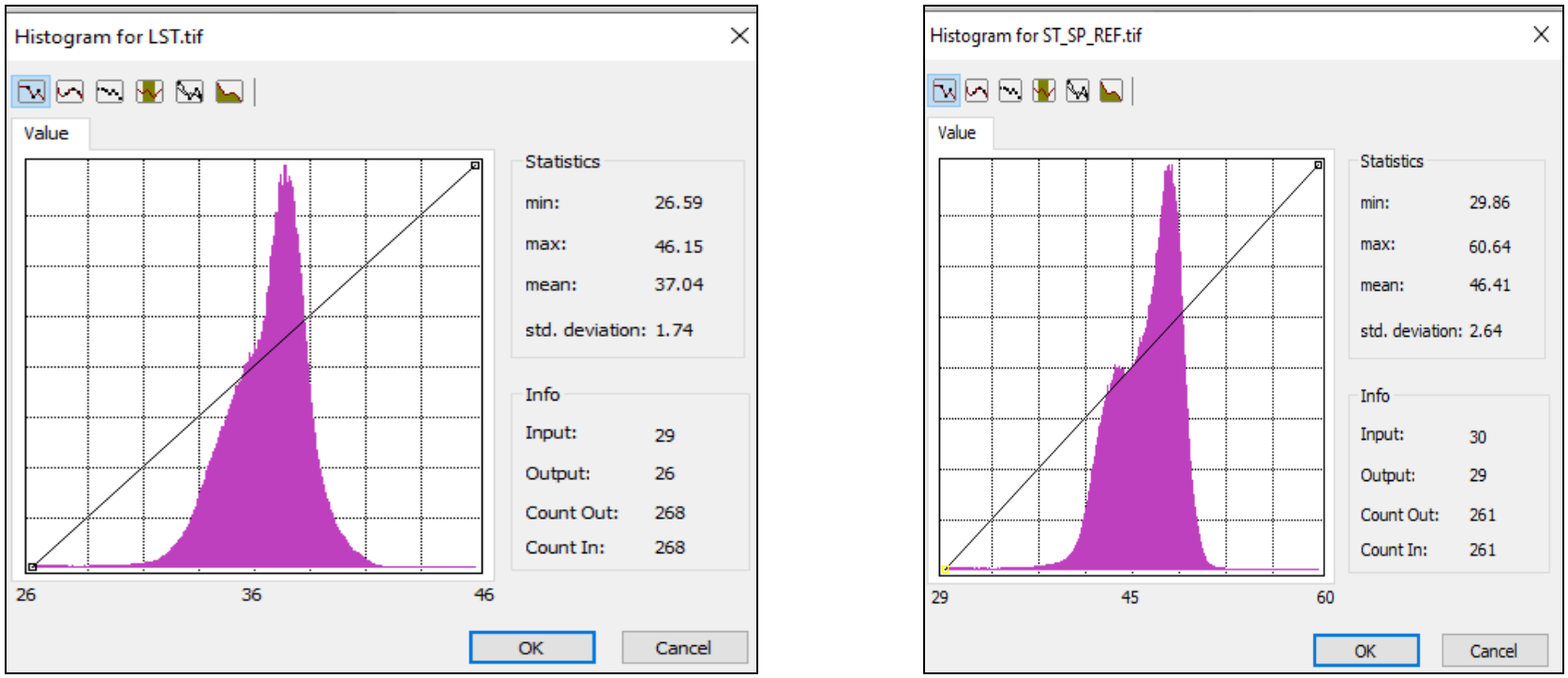

Fig. 11 A histogram illustrating the distribution pattern of variation in LST for C1 L1 and ST for C2 L2SP

Validation of LST with NDVI

Typically, vegetation has an impact on LST values. To investigate the relationship between LST and vegetation coverage in the study area, a statistical correlation was used, and the results are depicted in

Fig. 2. The plot illustrates that higher LST values, ranging from 36-45°C in C2L1 LST and 38-57°C in C2 L2SP ST images, are related to the NDVI range of 0.1 to 0.2, which corresponds to areas of the landscape such as urbanized regions, arid land, and rocky. In areas with vegetation cover, such as shrub and grassland, and water bodies of various depths, small LST results were observed (> 36°C in C2L1 LST and >45°C in C2 L2SP ST images). Although the relationship between LST and NDVI values is generally inverse, the research discovered a slight positive correlation between NDVI and LST in the presence of barren land and built-up areas in the image scene. It should be noted, however, that this trend is not consistent throughout the year and can vary depending on the season and time of day (Pal & Ziaul, 2017).

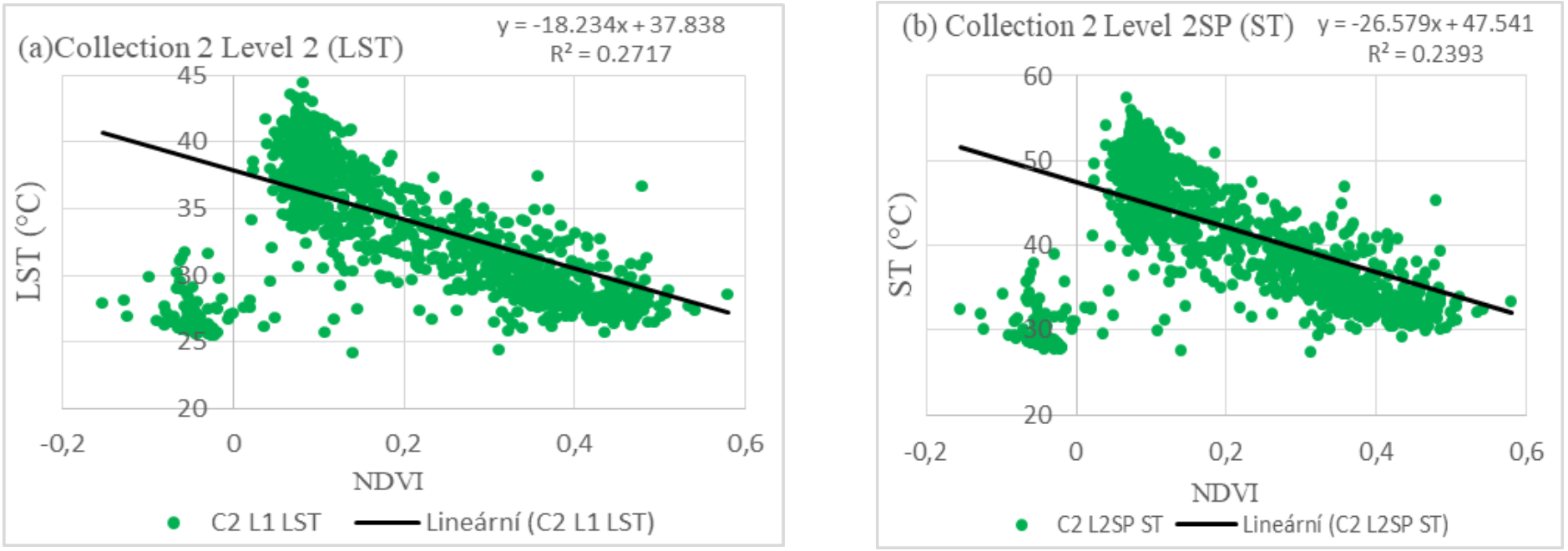

Fig. 12: Correlation between LST and NDVI: a) LST estimated from C2 L1 and b) ST estimated from C2 L2SP.

6. Conclusion

The Arc-UHI Toolbox offers an efficient and flexible method for estimating Land Surface Temperature (LST), Surface Temperature (ST), and Urban Heat Island (UHI) indices using Landsat collections (C2L1 and C2 L2SP). Developed using Python programming and ArcPy, the toolbox minimizes human error and reduces manual interventions, thereby accelerating the processing workflow. Validation with Landsat 9 C2 L2SP ST and NDVI data for identical 419 locations and times demonstrated consistent value ranges, patterns, and correlations, confirming 420 the accuracy of the estimated LST.

Future enhancements for the Arc-UHI Toolbox include expanding its capabilities to process data from other Landsat series, such as Landsat 5, 7, and 8, and reducing constraints on data usage. Additionally, broadening its applications to include satellite datasets with varying temporal and spatial resolutions, like Sentinel-2A (10 m) and ASTER (15 m), could provide more comprehensive insights. Incorporating additional automatic calculations, such as spectral reflectance-derived indices like the Normalized Difference Water Index (NDWI), Green Chlorophyll Index (GCI), Bare Soil Index (BSI), and Normalized Difference Soil Index (NDSI), could enhance the toolbox's functionality. These features could be organized into separate toolsets within the Arc-UHI Toolbox to further improve its utility.

The limitations of the current model include its reliance on Landsat 8 imagery, which may pose constraints in regions where only Landsat 5 or 7 images are available. Future research should focus on increasing the model's compatibility with these older Landsat series to enhance its applicability across various temporal and spatial contexts.

Acknowledgements

The authors express their gratitude to the USGS Earth Explorer website (earthexplorer.usgs.gov) for generously providing Landsat images for research purposes. They also extend their appreciation to all individuals who have contributed, either directly or indirectly to the research efforts.

Data Availability Statement

The article utilizes Landsat 8 level-1 products, which can be accessed and downloaded for preview from the USGS Earth Explorer Site EarthExplorer (usgs.gov). Once downloaded, the authors calibrated the raw data to obtain their results by running their code. The toolbox's source code is available on the figshare repository, and the private URL to access the code is provided on the following Github page: Arc-UHI-ToolBOX/ARC-UHI_TOOLBOX_pass.tbx at main · saraMsameh724/Arc-UHI-ToolBOX (github.com)

References

Abdullah, S., Barua, D., Abdullah, S. M. A., & Rabby, Y. W. (2022). Investigating the impact of land use/land cover change on present and future land surface temperature (LST) of Chittagong, Bangladesh. *Earth Systems and Environment*, 6(1), 221–235.

Abou El-Magd, I., Ismail, A., & Zanaty, N. (2016). Spatial variability of urban heat islands in Cairo City, Egypt using time series of Landsat Satellite images. *Int. J. Adv. Remote Sens. GIS*, 5, 1618–1638.

Abutaleb, K., Ngie, A., Darwish, A., Ahmed, M., Arafat, S., & Ahmed, F. (2015). Assessment of urban heat island using remotely sensed imagery over Greater Cairo, Egypt. *Advances in Remote Sensing*, 4(01), 35.

Clinton, N., & Gong, P. (2013). MODIS detected surface urban heat islands and sinks: Global locations and controls. *Remote Sensing of Environment*, 134, 294–304.

Duan, S.-B., Li, Z.-L., Zhao, W., Wu, P., Huang, C., Han, X.-J., Gao, M., Leng, P., & Shang, G. (2021). Validation of Landsat land surface temperature product in the conterminous United States using in situ measurements from SURFRAD, ARM, and NDBC sites. *International Journal of Digital Earth*, 14(5), 640–660.

Effat, H. A., Taha, L. G., & Mansour, K. F. (2014). Change detection of land cover and urban heat islands using multi-temporal landsat images, application in Tanta City, Egypt. *Open J Remote Sens Positioning*, 1(2), 1–15.

El-Zeiny, A. M., & Effat, H. A. (2017). Environmental monitoring of spatiotemporal change in land use/land cover and its impact on land surface temperature in El-Fayoum governorate, Egypt. *Remote Sensing Applications: Society and Environment*, 8, 266–277.

Guha, S., & Govil, H. (2020). Land surface temperature and normalized difference vegetation index relationship: a seasonal study on a tropical city. SN Applied Sciences, 2(10), 1–14.

Hidalgo García, D., & Arco Díaz, J. (2021). Spatial and Multi-Temporal Analysis of Land Surface Temperature through Landsat 8 Images: Comparison of Algorithms in a Highly Polluted City (Granada). *Remote Sensing*, 13(5), 1012.

Huang, Q., & Lu, Y. (2018). Urban heat island research from 1991 to 2015: a bibliometric analysis. *Theoretical and Applied Climatology*, 131(3), 1055–1067.

Hulley, G. C., Göttsche, F. M., Rivera, G., Hook, S. J., Freepartner, R. J., Martin, M. A., Cawse-Nicholson, K., & Johnson, W. R. (2021). Validation and quality assessment of the ECOSTRESS level-2 land surface temperature and emissivity product. IEEE Transactions on Geoscience and Remote Sensing, 60, 1–23.

Ihlen, V. (2019). *Landsat 8 data users handbook*. US Geological Survey: Sioux Falls, SD, USA, 55.

Jiang, Y., & Lin, W. (2021). A comparative analysis of retrieval algorithms of land surface temperature from Landsat-8 data: a case study of Shanghai, China. *International Journal of Environmental Research and Public Health*, 18(11), 5659.

Kafy, A.-A., Al Rakib, A., Akter, K. S., Rahaman, Z. A., Mallik, S., Nasher, N. M. R., Hossain, M. I., & Ali, M. Y. (2021). Monitoring the effects of vegetation cover losses on land surface temperature dynamics using geospatial approach in Rajshahi city, Bangladesh. *Environmental Challenges*, 4, 100187.

Kafy, A. Al, Faisal, A. Al, Rahman, M. S., Islam, M., Al Rakib, A., Islam, M. A., Khan, M. H. H., Sikdar, M. S., Sarker, M. H. S., Mawa, J., & Sattar, G. S. (2021). Prediction of seasonal urban thermal field variance index using machine learning algorithms in Cumilla, Bangladesh. *Sustainable Cities and Society*, 64, 102542. https://doi.org/10.1016/j.scs.2020.102542

Khan, F., Das, B., & Mishra, R. K. (2022). An automated land surface temperature modelling tool box designed using spatial technique for ArcGIS. *Earth Science Informatics*, 15(1), 725–733. https://doi.org/10.1007/s12145-021-00722-2

Kim, S.-M., Choi, Y., Suh, J., Oh, S., Park, H.-D., Yoon, S.-H., & Go, W.-R. (2012). ArcMine: A GIS extension to support mine reclamation planning. *Computers & Geosciences*, 46, 84–95.

Liu, X., Ming, Y., Liu, Y., Yue, W., & Han, G. (2022). Influences of landform and urban form factors on urban heat island: Comparative case study between Chengdu and Chongqing. *Science of the Total Environment*, 820, 153395.

Oguz, H. (2016). LST Calculator: A Python Tool for Retrieving Land Surface Temperature from Landsat 8 Imagery. Environmental *Sustainability and Landscape Management*, March 2013, 560–572.

Pal, S., & Ziaul, S. K. (2017). Detection of land use and land cover change and land surface temperature in English Bazar urban centre. *The Egyptian Journal of Remote Sensing and Space Science*, 20(1), 125–145.

Qin Z., Karnieli A., and Berliner P. (2001). A Mono-Window Algorithm for Retrieving Land Surface Temperature from Landsat TM Data and Its Application to the Israel-Egypt Border Region. International Journal of Remote Sensing, 18, 3719-3746.

Renard, F., Alonso, L., Fitts, Y., Hadjiosif, A., & Comby, J. (2019). Evaluation of the effect of urban redevelopment on surface urban heat islands. *Remote Sensing*, 11(3), 299.

Roupioz, L., Nerry, F., & Colin, J. (2018). Correction for the impact of the surface characteristics on the estimation of the effective emissivity at fine resolution in urban areas. Remote Sensing, 10(5), 746.

Sameh, S., Zarzoura, F., & El-Mewafi, M. (2023). Automated Mapping of Urban Heat Island to Predict Land Surface Temperature and Land use/cover Change Using Machine Learning Algorithms: Mansoura City. *International Journal of Geoinformatics*, 18(6). https://doi.org/https://doi.org/10.52939/ijg.v18i6.2461

Sobrino, J. A., Caselles, V., & Becker, F. (1990). Significance of the remotely sensed thermal infrared measurements obtained over a citrus orchard. *ISPRS Journal of Photogrammetry and Remote Sensing*, 44(6), 343–354.

Sobrino, J. A., Jiménez-Muñoz, J. C., & Paolini, L. (2004). Land surface temperature retrieval from LANDSAT TM 5. *Remote Sensing of Environment*, 90(4), 434–440.

Tucker, C. J. (1979). Red and photographic infrared linear combinations for monitoring vegetation. *Remote Sensing of Environment*, 8(2), 127–150.

United States Geological Survey (USGS). (n.d.-a). *Landsat Collections ensure that all Landsat Level-1 products contain known data quality.* https://www.usgs.gov/landsat-missions/landsat-collections

United States Geological Survey (USGS). (n.d.-b). *Using the USGS Landsat Level-1 Data Product.* https://www.usgs.gov/landsat-missions/using-usgs-landsat-level-1-data-product

Valor, E., & Caselles, V. (1996). Mapping land surface emissivity from NDVI: Application to European, African, and South American areas. *Remote Sensing of Environment*, 57(3), 167–184.

Vermote, E., Justice, C., Claverie, M., & Franch, B. (2016). Preliminary analysis of the performance of the Landsat 8/OLI land surface reflectance product. *Remote Sensing of Environment*, 185, 46–56.

Walawender, J., & Hajto, M. (2009). *Assessment of thermal conditions in urban areas with use of different satellite data and GIS*. 2009 EUMETSAT Meteorological Satellite Conference, Bath, UK, 21–25.

Walawender, J. P., Hajto, M. J., & Iwaniuk, P. (2012). *A new ArcGIS toolset for automated mapping of land surface temperature with the use of LANDSAT satellite data.* 2012 IEEE International Geoscience and Remote Sensing Symposium, 4371–4374.

Wang, H., Zhang, Y., Tsou, J. Y., & Li, Y. (2017). Surface urban heat island analysis of Shanghai (China) based on the change of land use and land cover. *Sustainability*, 9(9), 1538.

Wang, M., He, C., Zhang, Z., Hu, T., Duan, S.-B., Mallick, K., Li, H., & Liu, X. (2023). *Evaluation of Three Land Surface Temperature Products From Landsat Series Using in Situ Measurements*. IEEE Transactions on Geoscience and Remote Sensing, 61, 1–19.

Wulder, M. A., Loveland, T. R., Roy, D. P., Crawford, C. J., Masek, J. G., Woodcock, C. E., Allen, R. G., Anderson, M. C., Belward, A. S., & Cohen, W. B. (2019). Current status of Landsat program, science, and applications. *Remote Sensing of Environment*, 225, 127–147.

Wulder, M. A., Roy, D. P., Radeloff, V. C., Loveland, T. R., Anderson, M. C., Johnson, D. M., Healey, S., Zhu, Z., Scambos, T. A., & Pahlevan, N. (2022). Fifty years of Landsat science and impacts. *Remote Sensing of Environment*, 280, 113195.

Authors

[1] Sara Sameh - Public Works Engineering Department, Faculty of Engineering, Mansoura University, Mansoura 35516, Egypt;
Also Faculty of Engineering and Technology, Badr University in Cairo (BUC), Cairo, Egypt; sara.sameh@buc.edu.eg

[2] Fawzi Zarzoura - Public Works Engineering Department, Faculty of Engineering, Mansoura University, Mansoura 35516, Egypt

[3] Mahmoud El-Mewafi - Public Works Engineering Department, Faculty of Engineering, Mansoura University, Mansoura 35516, Egypt